Available online at www.sciencedirect.com
SCIENCE DIRECT®
Icarus 175 (2005) 92–110
ICARUS
www.elsevier.com/locate/icarus

Optical and thermal infrared observations of six near-Earth asteroids in 2002

Stephen D. Wolters [a,*], Simon F. Green [a], Neil McBride [a], John K. Davies [b]

[a] *Planetary and Space Sciences Research Institute, The Open University, Walton Hall, Milton Keynes, Buckinghamshire, MK7 6AA, UK*
[b] *Astronomy Technology Centre, Royal Observatory Edinburgh, Blackford Hill, Edinburgh EH9 3HJ, UK*

Received 3 June 2004; revised 20 September 2004

Available online 2 March 2005

Abstract

We present thermal infrared photometry and spectrophotometry of six Near-Earth Asteroids (NEAs) using the 3.8 m United Kingdom Infrared Telescope (UKIRT) together with quasi-simultaneous optical observations of five NEAs taken at the 1.0 m Jacobus Kapteyn Telescope (JKT). For Asteroid (6455) 1992 HE we derive a rotational period $P = 2.736 \pm 0.002$ h, and an absolute visual magnitude $H = 14.32 \pm 0.24$. For Asteroid 2002 HK_{12} we derive $H = 18.22$ $(+0.37, -0.30)$. The Standard Thermal Model (STM), the Fast Rotating Model (FRM) and the Near-Earth Asteroid Thermal Model (NEATM) have been fitted to the measured fluxes to derive albedos and effective diameters. The derived geometric albedos and effective diameters are (6455) 1992 HE: $p_v = 0.26 \pm 0.08$, $D_{\text{eff}} = 3.55 \pm 0.5$ km; 1999 HF_1: $p_v = 0.18 \pm 0.07$, $D_{\text{eff}} = 3.73$ $(+1.0, -0.5)$ km; 2000 ED_{104}: $p_v = 0.18 \pm 0.05$, $D_{\text{eff}} = 1.21 \pm 0.2$ km; 2002 HK_{12}: $p_v = 0.24$ $(+0.25, -0.11)$, $D_{\text{eff}} = 0.62 \pm 0.2$ km; 2002 NX_{18}: $p_v = 0.031 \pm 0.009$, $D_{\text{eff}} = 2.24 \pm 0.3$ km; 2002 QE_{15}: $p_v = 0.15$ $(+0.08, -0.06)$, $D_{\text{eff}} = 1.94 \pm 0.4$ km. The limitations of using the NEATM to observe NEAs at high phase angles are discussed.

Keywords: Asteroids; Infrared observations; Photometry; Spectrophotometry

1. Introduction

Over 2800 Near-Earth Asteroids (NEAs) have been discovered to date. On discovery of a NEA, the only physical parameter that is measured is its brightness at the phase angle at which it is observed. From this, the absolute visual magnitude H_v can be estimated by applying a correction to zero phase angle characterised by an assumed slope parameter, G (Bowell et al., 1989). The H magnitude alone does not provide a good constraint on an asteroid's diameter because its albedo can lie anywhere in the range 0.02–0.7. Fewer than 70 NEAs have reliably determined albedos and diameters to date.

Follow-up observations are required to determine further properties. The rotation period, rotation axis, shape constraints and phase curve can be determined from extended optical photometry. Thermal infrared spectrophotometry longer than 5 μm, combined with an appropriate thermal model and optical photometry, can be used to determine the asteroid's diameter and albedo. The albedo of an asteroid can constrain the taxonomic class and is vital for investigating the mineralogy. The size distribution and thermophysical properties of NEAs can help us to understand their evolution and the observed size distribution can be compared with the results of collisional evolution models. Size, shape and thermal properties can possibly distinguish the presence of extinct comets and can help constrain the Yarkovsky effect.

At the asteroid's surface, the incident solar flux is either scattered (proportional to diameter D^2 and albedo A) or absorbed (proportional to $D^2(1 - A)$). The scattered sunlight can be readily observed with optical photometry whereas the absorbed component is re-emitted at thermal infrared wavelengths. In principle, if we can measure the scattered light and the thermal infrared flux, a unique diameter and

* Corresponding author.
E-mail address: s.d.wolters@open.ac.uk (S.D. Wolters).

0019-1035/$ – see front matter
doi:10.1016/j.icarus.2004.10.013

albedo can be derived. However, we cannot directly measure the total radiation emitted in all directions and so a thermal model is needed to predict infrared flux received as a function of asteroid properties. We used three pre-existing thermal models to determine the diameters and albedos of the NEAs studied. The "refined" Standard Thermal Model (STM, Lebofsky et al., 1986) is a simple empirical model which assumes that an asteroid is a non-rotating spherical object with zero thermal inertia, and consequently there is no emission on the night side. It incorporates a beaming parameter, η, which takes account of enhanced sunward thermal emission at low phase angles due to surface roughness, and effectively also alters the temperature distribution to allow for the effects of rotation and thermal inertia. By calibrating their model to the main-belt Asteroids (1) Ceres and (2) Pallas, for which occultation diameters were available, Lebofsky et al. set $\eta = 0.756$. Following Lebofsky and Spencer (1989), the STM temperature distribution decreases from a maximum at the subsolar point to zero at the terminator:

$$T(\phi) = T_{\max} \cos^{1/4}\phi \quad \text{for } 0 \leqslant \phi \leqslant \pi/2, \tag{1}$$

where ϕ is the angle between the normal to the surface element and the asteroid–Sun vector. $T_{\max}$ is the subsolar maximum temperature ($T(\phi = 0)$) and is given by:

$$T_{\max} = \left[\frac{(1-A)S}{\eta\varepsilon\sigma}\right]^{1/4}, \tag{2}$$

where A is the bolometric Bond albedo, S is the incident solar flux, ε is the emissivity, for which a value of 0.9 is assumed, and σ is the Stefan–Boltzmann constant. The thermal flux is obtained by numerically integrating the Planck function at a given wavelength as a function of $T(\phi)$ over the visible hemisphere, the dimensions of which depend on the diameter. The absolute visual magnitude, from optical photometry, allows a unique diameter (D) to be calculated for a given albedo using the following expression (e.g., Fowler and Chillemi, 1992):

$$D(\text{km}) = 10^{-H/5} 1329/\sqrt{p_v}, \tag{3}$$

where p_v is the visual geometric albedo. $p_v = A/q$ where q is the phase integral which is related to G (Bowell et al., 1989). Since the STM is defined at zero phase, a crude phase angle correction of 0.01 mag deg^{-1}, which is considered to be valid for phase angles less than 30° (e.g., Morrison, 1977), is applied to the thermal IR photometry. The STM provides accurate diameters and albedos for main-belt asteroids, for which the assumptions of the model are reasonable, since they are likely to have a dusty regolith with a low thermal inertia, are observed at low phase angles and rotate slowly.

The second model used is the Fast Rotating Model (FRM, Lebofsky and Spencer, 1989), also known as the isothermal latitude model. This can be regarded as the opposite extreme to the STM; the surface temperature distribution depends only on latitude, and the day and night side are at an equal temperature. The FRM applies to an asteroid that has a high thermal inertia (e.g., one with exposed bare rock) and/or fast rotation.

The STM and the FRM can be used to fit thermal models to a single broadband thermal infrared measurement, e.g., the N-band centred at 10.5 μm, although multi-wavelength data are required to determine the applicability of either. Neither the STM nor the FRM provide accurate diameters for many NEAs (e.g., Veeder et al., 1989). NEAs tend to be smaller and more irregular than main-belt asteroids, and are often observed at large phase angles. Ideally, a full thermophysical model, taking account of the non-spherical shape, rotation properties and conduction into or out of the surface to derive the emission from each surface element, should be used to predict the thermal emission. In practice, most or all of these properties are unknown, but some refinements to the STM/FRM can be made. Harris (1998) introduced the Near-Earth Asteroid Thermal Model (NEATM), an empirical model which makes two changes to the STM. First, it allows the beaming parameter η to be treated as a calibration parameter; for multi-wavelength data it is varied to give the best fit. This is equivalent to adjusting the model temperature distribution to be consistent with the observed thermal flux. If insufficient measurements at a great enough range of wavelengths are available, or the quality of the data is inadequate, then default values of η can be used. Delbó et al. (2003) suggested using $\eta = 1.0$ for $\alpha < 45°$ and $\eta = 1.5$ for $\alpha > 45°$ based on a trend of increasing η with phase angle. Second, it introduces a phase angle correction by modelling the asteroid as a sphere and calculating numerically the thermal emission from the surface of the asteroid which is in sunlight and visible to the observer. It assumes Lambertian emission and that there is no emission on the night-side, as would be the case for slow-rotating, low thermal inertia objects.

2. Observations and data reduction

2.1. Optical observations

Observations of Asteroids (6455) 1992 HE, 2000 ED_{104}, 2002 HK_{12}, 2002 NX_{18}, and 2002 QE_{15} were carried out at the 1.0 m Jacobus Kapteyn Telescope (JKT) between 25 September and 1 October 2002 UT, using the SITe2 CCD camera fitted with a 2000 × 2000 pixel chip with 0.33″ resolution in the V filter. The observational circumstances are shown in Table 1. The telescope was tracked at the sidereal rate for the observations, but exposures were limited to 8, 30, 40, and 35 s for (6455) 1992 HE, 2000 ED_{104}, 2002 NX_{18}, and 2002 QE_{15} respectively so that the image did not trail by more than 1.5 pixels. Circular apertures could then be fitted onto the object and comparison stars. Small (1.7 FWHM diameter) and large (5.1 FWHM diameter) apertures were used on each frame. The small aperture was sufficiently large to sample most of target point spread function, but as

Table 1
Observational geometry

Object	UT date	R (AU)	Δ (AU)	$\alpha°$	Comments
(6455) 1992 HE	2002-03-22	1.647	0.745	22	UKIRT N and Q photometry
	2002-09-28	1.352	0.444	32	JKT V photometry, UKIRT N spectrum
	2002-09-29	1.360	0.444	30	JKT V photometry
	2002-09-30	1.367	0.444	29	JKT V photometry, UKIRT N and Q spectra
	2002-10-02	1.383	0.447	26	JKT V photometry
1999 HF_1	2002-03-22	0.958	0.207	95	UKIRT N and Q photometry
2000 ED_{104}	2002-09-29	1.090	0.209	60	UKIRT N spectrum
	2002-09-30	1.085	0.199	60	UKIRT N spectrum
	2002-10-01	1.080	0.189	61	JKT V photometry
2002 HK_{12}	2002-09-28	1.138	0.169	34	UKIRT N spectrum
2002 NX_{18}	2002-09-25	1.158	0.284	51	JKT V photometry
	2002-09-27	1.154	0.282	51	JKT V photometry, UKIRT N spectrum
	2002-09-28	1.145	0.277	53	JKT V photometry
	2002-09-29	1.145	0.277	53	JKT V photometry, UKIRT N spectrum
	2002-09-30	1.141	0.274	53	UKIRT N and Q spectra
	2002-10-01	1.133	0.269	55	JKT V photometry
2002 QE_{15}	2002-09-28	1.132	0.420	62	JKT V photometry, UKIRT N spectrum

Notes. Ephemerides are taken from JPL Horizons, and are at 0hUT on the night of observation.

small as possible to minimise the sky contribution, as discussed in Green and McBride (1998). Instrumental magnitudes were measured with the Starlink photometry software GAIA, except for 2002 HK_{12} where MaxIm DL 4 was used. We used a sky background annulus of 1.7–2.5 × the aperture radius for the large aperture and 5.1–7.5 × the aperture radius for the small aperture in order to use the same area of sky background for both aperture sizes. The observations were bias-corrected using an over-scan region on the CCD, and flat-fielded using defocused images of the uniformly illuminated dome interior, using the Starlink software packages KAPPA and Figaro. Conditions were photometric for much of 25, 27, and 28 September; standard stars taken from Landolt (1992) were used for photometric calibration using the large aperture. Lightcurves relative to comparison stars on the field were obtained; as the field shifted new comparison stars were used. A relative lightcurve for the whole night was obtained by cross-calibration. Apparent magnitudes were produced through photometric calibration of the comparison "star." Reduced magnitudes $V(1,\alpha)$ were derived using the observational geometry obtained from JPL Horizons (Table 1) (http://ssd.jpl.nasa.gov/horizons.html).

2.2. Thermal infrared photometry March 2002

Observations were made on 22 March 2002 (UT) under clear skies at the United Kingdom Infrared Telescope (UKIRT). Michelle is a mid-infrared imager/spectrometer with a SBRC Si:As 320 × 240-pixel array operating between 8 and 25 μm. When used in imaging mode it provides 67.2 × 50.4 arcsec field of view at 0.21 arcsec per pixel. Images were taken using the standard UKIRT imaging sequences which include nodding and chopping. The result is a final frame with four images, two positive and two negative, resulting from the sum of the chopped pairs at the first nod position, plus the second chopped pairs at the opposite nod. These images were pipeline reduced by the Observatory Reduction and Acquisition Control Data Reduction (ORAC-DR) package, developed at the Joint Astronomy Centre, which 'snips' the images, inverts them as needed, and then recombines them as a single frame, one quarter of the size of the array, containing a single positive image comprising the sum of the four nod-chop positions.

Photometry was carried out on these images using the photometry module of Starlink GAIA software. An aperture of 13 pixels radius (equivalent to a 5.5 arcsec diameter) was used for determining the flux from the object. This aperture includes the central spot plus the first diffraction ring. Since the background sky is removed by the chopping, it should not be necessary to subtract the sky background but as a precaution a sky annulus of from 19.5 to 30 pixels was used to remove any residual background.

Determination of the extinction and photometric calibration was done in the normal manner using the following stars: BS 2990, BS 3748, and BS 5340 for the 18.5 μm filter, BS 5340, BS 5793, and BS 7525 for the 10.3 and 12.5 μm filter and those plus BS 6134 for the 8.8 μm filter. Standard star magnitudes were derived from the MIRAC manual, the Timmi2 website (http://www.ls.eso.org/lasilla/sciops/3p6/timmi) and the IRTF-ISO (http://irtfweb.ifa.hawaii.edu/IRrefdata/Catalogs/bright_standards) website.

2.3. Thermal infrared spectrophotometry September 2002

Observations in the thermal infrared were carried out at UKIRT on five half-nights in September 2002 using the Michelle instrument in spectroscopy mode, in which it has a resolution of 0.38 arcsec per pixel. The observational cir-

cumstances are shown in Table 1. The weather on 27, 28, and 30 September UT appeared to be clear with the atmospheric absorption coefficient $\tau = 0.14$ on 27 and 28 September, and $\tau = 0.07$ on 30 September. On 29 September, about 5/8 fraction of the sky was covered with cirrus. Typical seeing was about 0.5″.

The lowN and lowQ gratings were used, obtaining spectra in the range 7–12.5 and 17–25 μm, respectively. The gratings can be set to different slit widths: on 27, 28, and 30 September a 4-pixel slit width was used to maximise the accuracy of the absolute flux-calibration by ensuring that all the possible light from the ratio star was received. On 29 September a 2-pixel slit was used so as to reduce noise from the sky background due to the cirrus. During an observation the telescope was "chopped" with an amplitude of 16″ and frequency 10 Hz in a direction along the slit. Chopping allows us to use off-source exposures to remove the effects of atmospheric emission from the spectrum; chopping along the slit maximises the observing time on the target since the source is always being measured. The cancellation tends to be effective as long as the chop frequency is higher than the characteristic timescale over which the sky emission changes. The telescope was also "nodded," by beamswitching, where the chop positions of the target and the sky are swapped. Nodding removes the effect from the changing thermal emission due to the telescope optics as the telescope is chopped. The timescale for nodding can be longer than that for chopping because its effectiveness depends on the more slowly varying parameters along the telescope's optical path. The observing sequence is "on-source," "off-source," "off-source," "on-source," so that each output frame thus consists of four horizontal rows (several pixels wide), with off-source rows apparent as negative values on the image. The on-source and off-source rows are overlaid in a group file formed for each observing sequence. The group file has bad pixels masked and is bias-corrected; it is then flat-fielded using an image taken with a flat-fielding plate at the beginning of the night. The rows are then optimally extracted and coadded to produce a final spectrum. Fuller details on the instrument can be found on the Joint Astronomy Centre website (http://www.jach.hawaii.edu/JACdocs/UKIRT/michelle/michelle_atc/user/ocdd/ocdd.html).

Ephemerides for each target were obtained from JPL's Horizons System, and the telescope was tracked at the rates provided while offset autoguiding on a nearby star.

The raw data were flux-calibrated using ORAC-DR, which automatically performs the coadding and other data reduction described above on the group image containing the four horizontal on- and off-source rows. It optimally extracts the spectrum of the row to be coadded using the Starlink Figaro routine OPTEXTRACT. The ORAC-DR code was adapted so that the optimal extraction window centre (the row containing the peak flux) and width could be manually selected for each observation group. An optimal extraction window of 3 or 4 pixels wide (0.64″ and 0.85″, respectively) was found to yield the most favourable signal-to-noise ratio and both were subsequently used.

A ratio star for each object (asteroid) was used to correct for wavelength-dependent atmospheric transmission. Bright ratio stars, of spectral type K0 and earlier with smooth spectra (no SiO fundamental band), were chosen to be close on the sky to the object and at as similar an airmass as possible. The ratio star spectrum is divided by a black-body profile using a temperature appropriate for the spectral type of the star, in order to remove the spectral shape of the ratio star. The object spectrum is then divided by the normalised ratio star spectrum.

For flux-calibration a standard star with known N- and Q-band flux was observed, several times throughout the night if possible. Absolutely calibrated infrared N- and Q-band fluxes were taken from Tokunaga (1984) and Rieke et al. (1985). Using the filter-instrument profile given by Tokunaga (2000), integrated absolute fluxes for the standard stars were obtained. If a standard star close enough to the object in the sky has been observed, then it can be used as the ratio star as well. In this case, the ratio of the object's raw counts was multiplied by the integrated absolute flux of the standard star to obtain a flux-calibrated spectrum (for all Q-band measurements, a standard star was used directly for flux-calibration). Otherwise, the ratio star itself was flux-calibrated, by taking the ratio of the observed raw counts of the two stars. The differing atmospheric extinction between the ratio star and the standard star was accounted for using a mean IR extinction correction for UKIRT of $k_N = 0.151$ mag airmass^{-1} (http://www.jach.hawaii.edu/JACpublic/UKIRT/astronomy/exts.html). Using separate ratio and standard stars instead of standard stars alone has the advantage that a ratio star for correction of atmospheric transmission could be chosen closer in the sky to the asteroid, since there were more stars to choose from, but there is additional error introduced by the need to flux-calibrate the ratio star.

Wavelength calibration was carried out by using sky-arcs for each observation group, generated by co-adding the chop beams, and calibrating to model atmosphere spectra.

The raw spectra in the N- and Q-filters covered between 8–12.5 and 18–25 μm respectively with a resolution of about 0.03 μm per pixel (the dispersion was non-linear). The N-filter spectra were binned over wavelength ranges varying between 0.26 μm (10 pixels) and 1.53 μm (51 pixels) depending on the data quality for that object at that wavelength. The flux measured in the atmospheric ozone absorption feature at 9.3–10 μm is excluded. The Q-filter spectra were binned over wavelength ranges between 0.75 μm (25 pixels) and 1.62 μm (54 pixels). They were also binned for more accurate flux measurements between 17.4 and 18.8 μm where the best signal to noise ratio is obtained due to low atmospheric absorption.

The wavelength-dependent error contributed by differing atmospheric absorption between the ratio star and the object was estimated for each night by dividing a bright standard

star's spectrum with two different ratio stars' spectra at different airmasses, then taking the ratio of the two measured fluxes for the standard star. The resulting scatter at different wavelengths is due solely to the differing atmospheric absorption from using ratio stars at different airmasses and at different parts of the sky; it was found to be between 1 and 3% for the N-band between 8–9.3 and 10.0–12.5 μm (the data from the ozone absorption band 9.3–10.0 μm were excluded) but would be smaller for our targets because the airmass differences between the asteroids and the ratio stars were smaller. The error bars on the binned fluxes represent the statistical standard error on the mean of the binned fluxes only. There is additional uncertainty in absolute calibration, partly due to imperfectly accounting for differing atmospheric absorption between the standard star and object. This was estimated by treating a bright standard star (BS 7001, Vega) as if it were a target asteroid, flux calibrating it using another standard star at a different airmass, and then comparing its measured N magnitude with its known magnitude. This was found to be typically 4% different. There is further uncertainty in the absolute calibration due to electronic pickup, a poorly understood source of noise in the array; it appears to be much more extensive on 27, 28, and 30 September, compared to 29 September UT. This results in a horizontal rippling effect in the group image which has a greater percentage effect on the absolute flux calibration the fainter the object being observed. For (6455) 1992 HE on 28 and 30 September UT and 2002 NX_{18} on 27 and 30 September this is estimated to introduce no more than a 5% error in the absolute flux calibration. However, for 2000 ED_{104} on 30 September, and 2002 QE_{15}, the error may be as large as 30%, and for 2002 HK_{12} up to 50%. The effect on the uncertainty in the estimation of $D_{\rm eff}$ scales as the square root of the above uncertainty and is discussed in Section 4, and the effect on the uncertainty of η is negligible since the shape of the spectrum is not affected. On 29 September the electronic pickup is negligible.

3. Results and data analysis from optical observations

3.1. (6455) 1992 HE

Asteroid (6455) 1992 HE was observed on the nights of 27, 28, 29 September and 1 October. We obtained a rotational period $P = 2.736 \pm 0.002$ h from a 6th order Fourier fit of all four nights' data, allowing an arbitrary absolute shift in mean magnitude between each night (i.e., treating each night as a relative lightcurve). Figure 1(a) shows a composite lightcurve, with the mean magnitudes of 29.1, 30.1 September UT and 2.1 October UT shifted to coincide with that of 28.2 September UT. We measured a reduced visual mean magnitude $V(1, \alpha = 33.0^\circ) = 15.42 \pm 0.02$ with a lightcurve amplitude of 0.21, where the uncertainty results from an estimate of the reliability of the absolute calibration on the night of 27 September. Using a slope parameter of $G = 0.34 \pm 0.1$ from Pravec (personal communication, 2003) we derive an absolute visual magnitude H of 14.32 ± 0.24, where the uncertainty is dominated by the correction to zero phase due to the uncertainty in the slope parameter G.

3.2. 2000 ED_{104}

Limited relative optical photometry of 2000 ED_{104} obtained on October 1 shows that the lightcurve amplitude is > 1 mag and that the rotational period P is $\gg 3.8$ hours (Fig. 1(b)).

3.3. 2002 HK_{12}

2002 HK_{12} was observed on the nights of 25, 26, and 27 September. Unfortunately there were not enough observations to create a composite lightcurve. Pravec (personal communication, 2004, see http://www.asu.cas.cz/~ppravec/newres.htm) observed the asteroid between 7 and 12 September and found the rotational period to be $P = 12.691 \pm 0.003$ h and a lightcurve amplitude of 1.5 mag (at a phase angle of 78°, so the amplitude has probably been affected by the amplitude-phase effect). A 6th order Fourier fit with this period was applied to our data and can be seen in Fig. 1(c). We measured a reduced visual mean magnitude $V(1, \alpha = 33.6^\circ) = 19.62 \pm 0.02$. Assuming a slope parameter of $G = 0.15$ $(+0.25, -0.15)$ we derive an absolute visual magnitude of $H = 18.22$ $(+0.37, -0.30)$. The midpoint of the thermal IR observation of 2002 HK_{12} is at 0.38 rotational phase, in the range not covered by our data. Examination of Pravec's lightcurve allows us to extrapolate to 0.38 rotational phase symmetrically with the other lightcurve maximum, which is covered by our data, with an additional uncertainty of 0.1 mag. The absolute visual magnitude used for the radiometric diameter and albedo derivation is near lightcurve maximum, $H = 17.67$ $(+0.38, -0.31)$.

3.4. 2002 NX_{18}

2002 NX_{18} was observed on the nights of 25, 27, 28, 29 September and 1 October. The lightcurve coverage was not adequate to produce a unique solution for the rotational period. The two best solutions are shown in Figs. 1(d) and 1(e), obtained from a 4th order Fourier fit, allowing for an arbitrary shift in mean magnitude to coincide with that of 27.9 September UT. The two best solutions are $P = 7.602 \pm 0.002$ h and $P = 9.040 \pm 0.002$ h. Assuming the $P = 9.040$ h solution is correct, we measured a reduced visual mean magnitude $V(1, \alpha = 51.9^\circ) = 19.54 \pm 0.02$ with a lightcurve amplitude of 0.23 (the $P = 7.602$ h solution gives the same V with a lightcurve amplitude of 0.22). Assuming a slope parameter of $G = 0.15$ (a typical value of G for a low-albedo C-type object) we derive an H magnitude of 17.63 ±0.5 (the large uncertainty due to G being totally unknown).

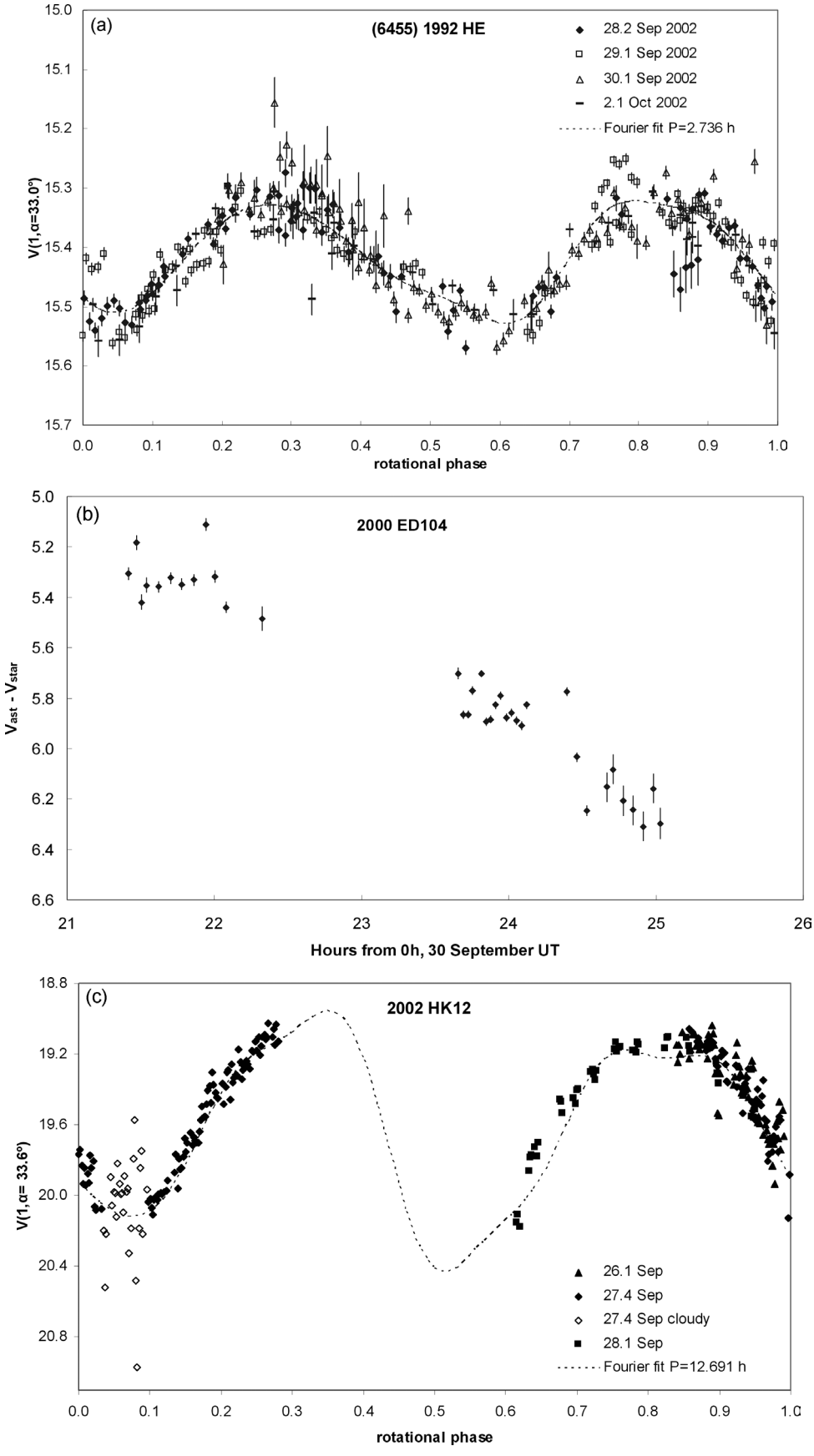
(a)
(6455) 1992 HE
28.2 Sep 2002
29.1 Sep 2002
30.1 Sep 2002
2.1 Oct 2002
Fourier fit P=2.736 h
V(1,α=33.0°)
rotational phase
(b)
2000 ED104
V_ast - V_star
Hours from 0h, 30 September UT
(c)
2002 HK12
26.1 Sep
27.4 Sep
27.4 Sep cloudy
28.1 Sep
Fourier fit P=12.691 h
V(1,α= 33.6°)
rotational phase

Fig. 1.

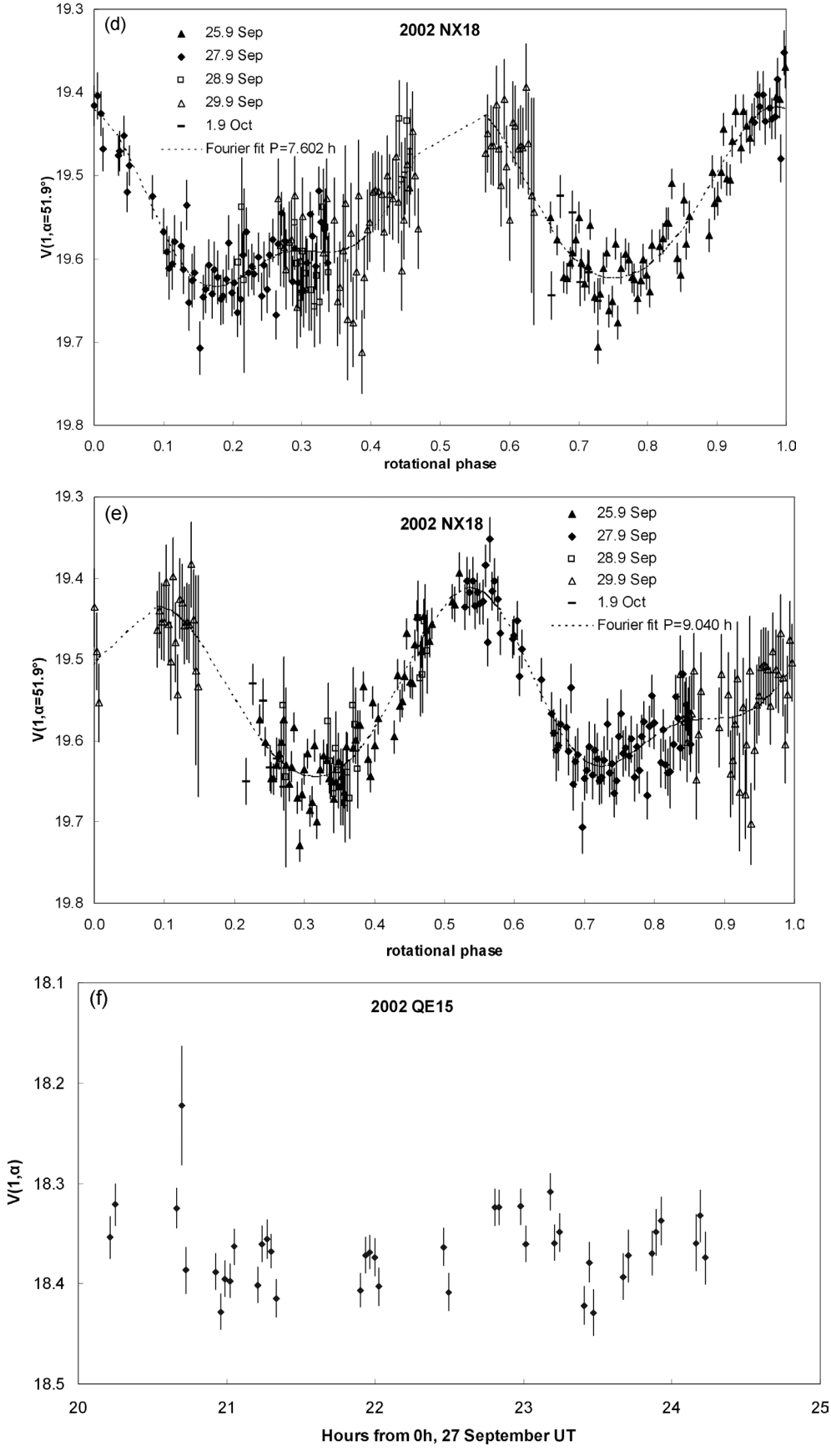

Fig. 1. Continued.

3.5. 2002 QE_{15}

Pravec (personal communication, 2003), from observations on 30 September to 2 October 2002, found a rotational period for 2002 QE_{15} of 2.5811 ± 0.0001 h assuming the second harmonic in the Fourier fit is dominant, and a lightcurve amplitude of 0.09. Because the lightcurve amplitude is low the period may have more than the usual two extremes per cycle, due, for example, to local topography or albedo variations on the surface. We obtained limited optical photometry of 2002 QE_{15} on 28 September for 3.1 h (Fig. 1(f)) and found no variation greater than 0.12 mag. Using our mean $V(1, \alpha = 61.7^\circ) = 18.37 \pm 0.02$ mag, and assuming $G = 0.15$, we derive an H magnitude of 16.17 ± 0.5 which is in close agreement to the catalogued value at JPL Horizons of $H = 16.21$ that we used for the thermal model fitting for this asteroid.

4. Results and data analysis from thermal infrared observations

Figure 2 shows the binned spectra for the six asteroids observed at UKIRT in March 2002 and September 2002, with the best-fit STM, FRM and NEATM thermal models. Table 2 shows the corresponding effective diameters $D_{\rm eff}$ (the diameter the asteroid would have if it was a perfect sphere) and geometric albedos p_v, as well as the H_v magnitude used. The adopted results column in Table 2 shows the final result arrived at in the discussions about each individual object below; for those objects where multiple spectra are available ((6455) 1992 HE, 2000 ED_{104}, and 2002 NX_{18}) this is an average of the reliable spectra shown in bold, for 1999 HF_1 this is an average of the FRM and the NEATM fits, whereas for the other objects where there was only one spectrum this is simply the NEATM fit for that object.

The uncertainty in the model fitting typically dominates the uncertainty in the flux calibration and the scatter due to atmospheric absorption discussed in Section 2.3. Comparison with other sources such as radar shows that it is generally less than 15% in diameter and 30% in albedo. In the cases of 2002 QE_{15} and 2002 HK_{12}, the observational uncertainties are of the same order of magnitude as the uncertainty due to model-fitting because of the electronic pickup problem. For these asteroids, the uncertainty in the adopted result is calculated from the change in the albedo and diameter from the NEATM fit obtained at either end of the possible range of calibrated fluxes, combined with the model fitting uncertainty. For 2000 ED_{104} the uncertainty in the adopted result reflects a large H_v uncertainty estimated at ± 0.5 due to a large lightcurve amplitude of greater than 1 mag. For 1999 HF_1 the uncertainty is bounded by the NEATM and FRM fits.

Many previous derivations of albedo and diameter using NEATM fitting have used measurements over the range 4–20 μm from instruments such as the Keck I/Long Wave Spectrometer (e.g., Delbó et al., 2003) or non-simultaneous narrow-band photometry (e.g., Harris et al., 1998). Although the Michelle spectra, in both the Q- and the N-band, are able to produce higher spectral resolution in the ranges covered, there are no data at wavelengths shorter than 8 μm. The greater the wavelength range available the more accurately the shape of the thermal infrared spectra can be fitted and the models are particularly sensitive in the 5 μm (M-band) region. Where only N-band data for an object are available, the accuracy of the NEATM fitted η is hard to gauge, since there are not generally enough results to judge the reproducibility. In the cases of Asteroids (6455) 1992 HE and 2002 NX_{18} where N- and Q-band data are available, combined with a high spectral resolution in the 7–12.5 μm region, and where closely reproduced best-fit η are found on different nights, the NEATM fitted η are certainly reliable enough to use the uncertainties associated with the model discussed above.

For 1999 HF_1, 2000 ED_{104}, 2002 NX_{18}, and 2002 QE_{15} the accuracy of the measured diameters and albedos are dominated by the uncertainty in their corresponding H magnitude, due to a combination of optical observations at high phase angle and an unknown phase parameter. A change of H by $+0.3$ mag produces a change in modelled diameter of $\sim -15\%$ and modelled geometric albedo of $\sim +30\%$. In the future, when knowledge of these objects visual magnitude, and/or phase parameter improves, the albedo and diameter can be updated using the helpful expressions given by Harris and Harris (1997).

A value of $G = 0.15$ is assumed for all the thermal model fitting, except for (6455) 1992 HE where $G = 0.34$ is used.

4.1. (6455) 1992 HE

Figure 2(a) shows the thermal model fits to (6455) 1992 HE March 2002 infrared photometry. Figures 2(b) and 2(c) show fits to N-band spectra from September 28 and 30, respectively. Figures 2(d) and 2(e) show the 30 September N-band spectrum combined with the first Q-band spectrum

Fig. 1. (a) Composite visual lightcurve of Asteroid (6455) 1992 HE with 6th order Fourier fit of rotational period $P = 2.736$ h. Mean magnitudes of 29.1, 30.1 September and 2.1 October UT are shifted to agree with 28.2 September UT, when the weather was photometric. There was cirrus on 30 September and 2 October for some of the coverage. Error bars represent the statistical uncertainties in the photometry. The absolute magnitude, as measured by the 28.2 September data, is additionally uncertain by 0.02 mag from the scatter of the atmospheric extinction curve, and there are also uncertainties resulting from chip errors and flat-fielding errors. (b) Relative visual lightcurve of 2000 ED_{104} taken between 30.9 September and 1.0 October UT. (c) Composite visual lightcurve of 2002 HK_{12} with 6th order Fourier fit of rotational period $P = 12.691$ h. (d) Composite visual lightcurve of 2002 NX_{18} with 4th order Fourier fit of rotational period $P = 7.602$ h, errors as in (a). (e) Composite visual lightcurve of 2002 NX_{18} with 4th order Fourier fit of rotational period $P = 9.040$ h, errors as in (a). (f) Reduced magnitude visual lightcurve of 2002 QE_{15} taken between 27.8 and 28.0 September UT. Zero rotational phase is at 0 h, 25 September UT for (a), (c), (d), and (e).

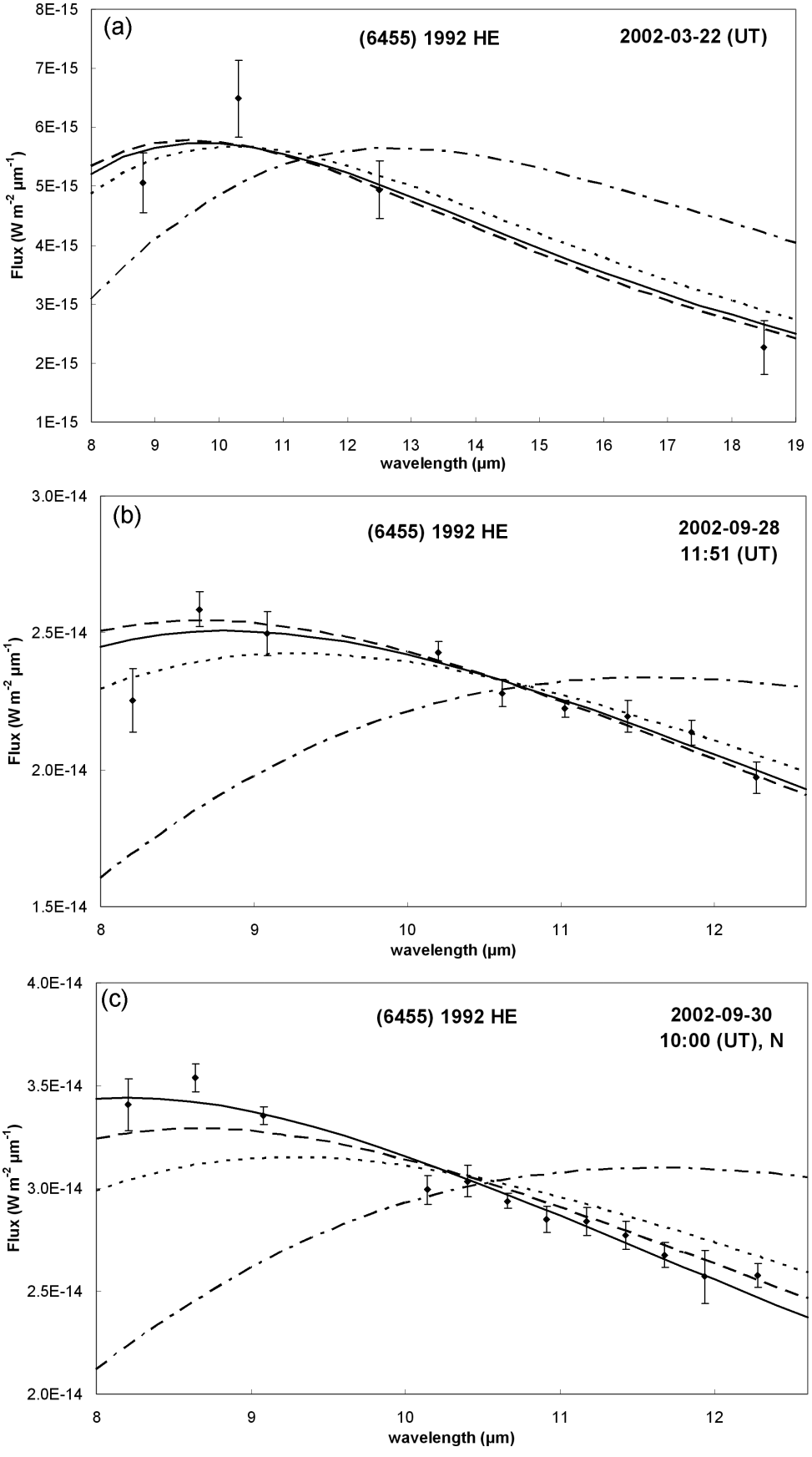
(a)
(6455) 1992 HE
2002-03-22 (UT)
Flux (W m-2 µm-1)
wavelength (µm)
(b)
(6455) 1992 HE
2002-09-28
11:51 (UT)
Flux (W m-2 µm-1)
wavelength (µm)
(c)
(6455) 1992 HE
2002-09-30
10:00 (UT), N
Flux (W m-2 µm-1)
wavelength (µm)

Fig. 2.

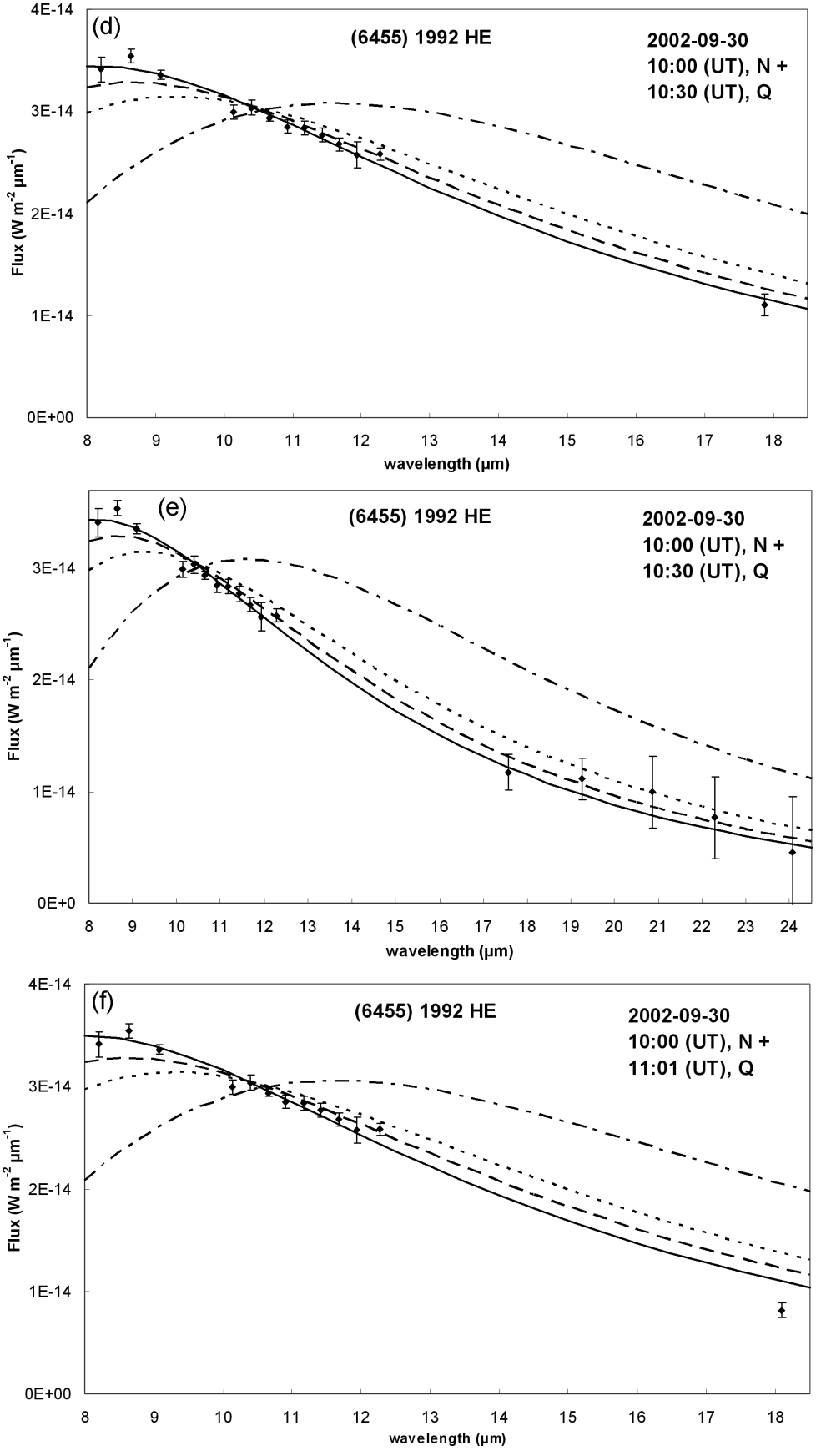

Fig. 2. Continued.

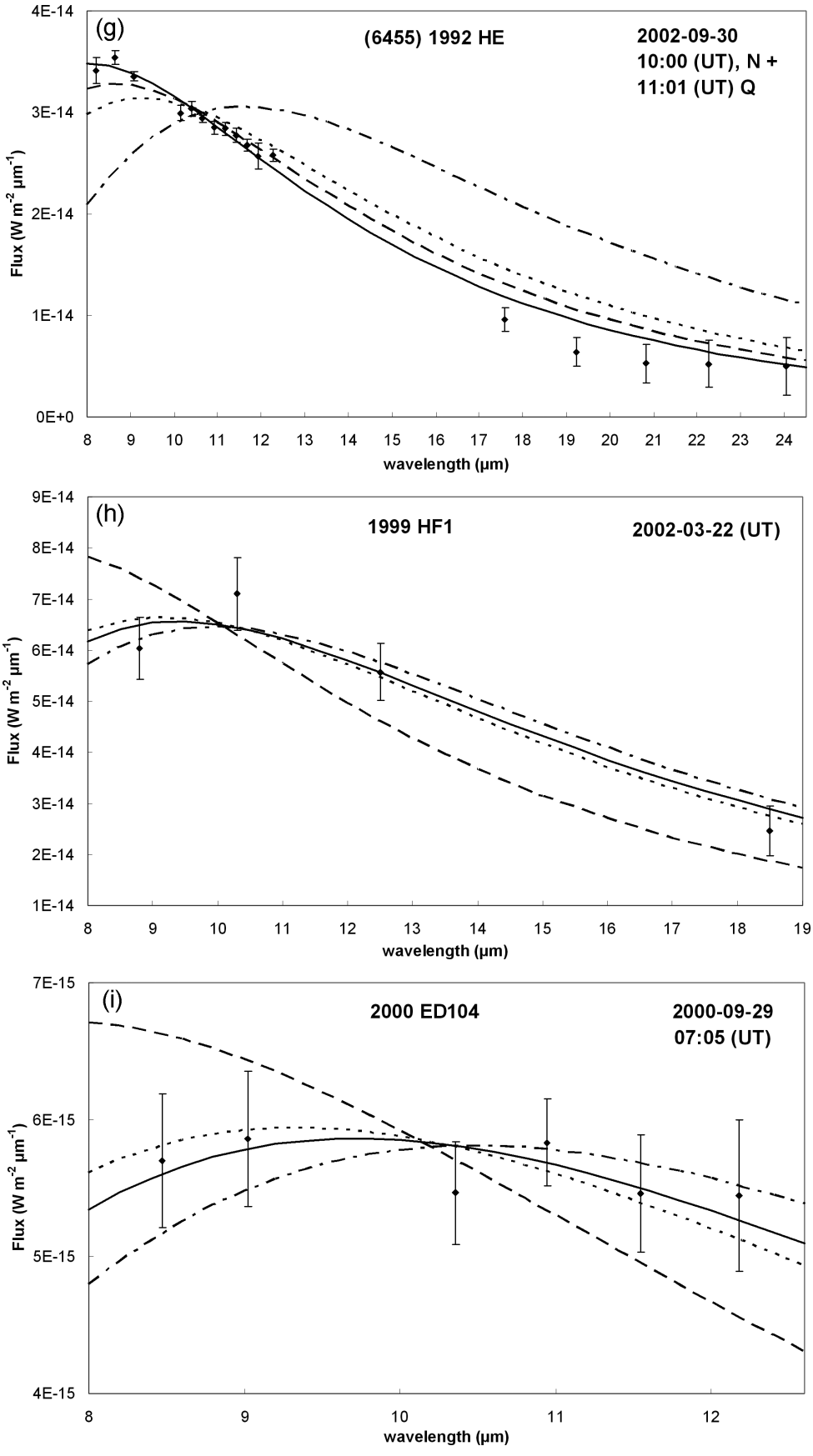

Fig. 2. Continued.

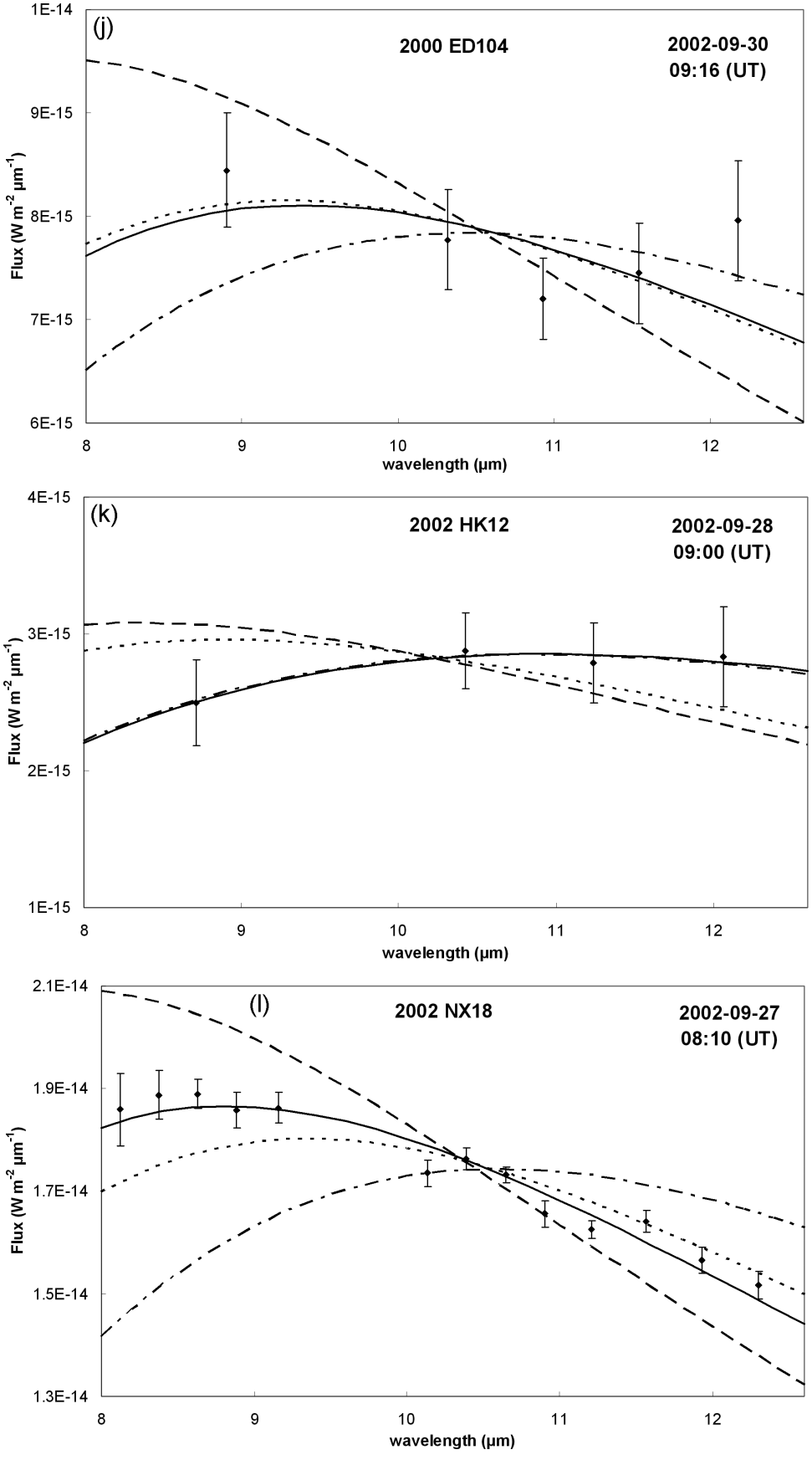

Fig. 2. Continued.

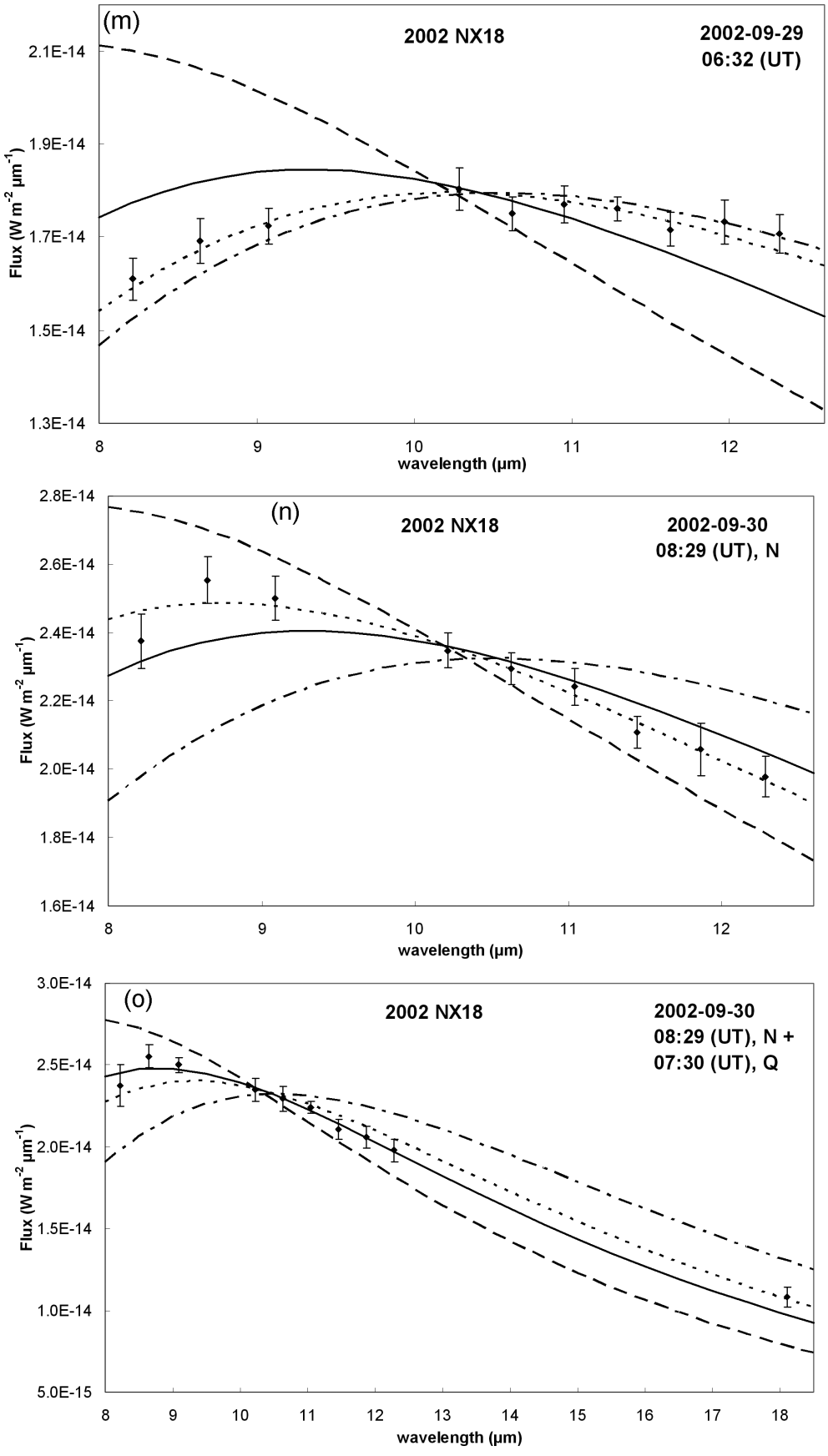

Fig. 2. Continued.

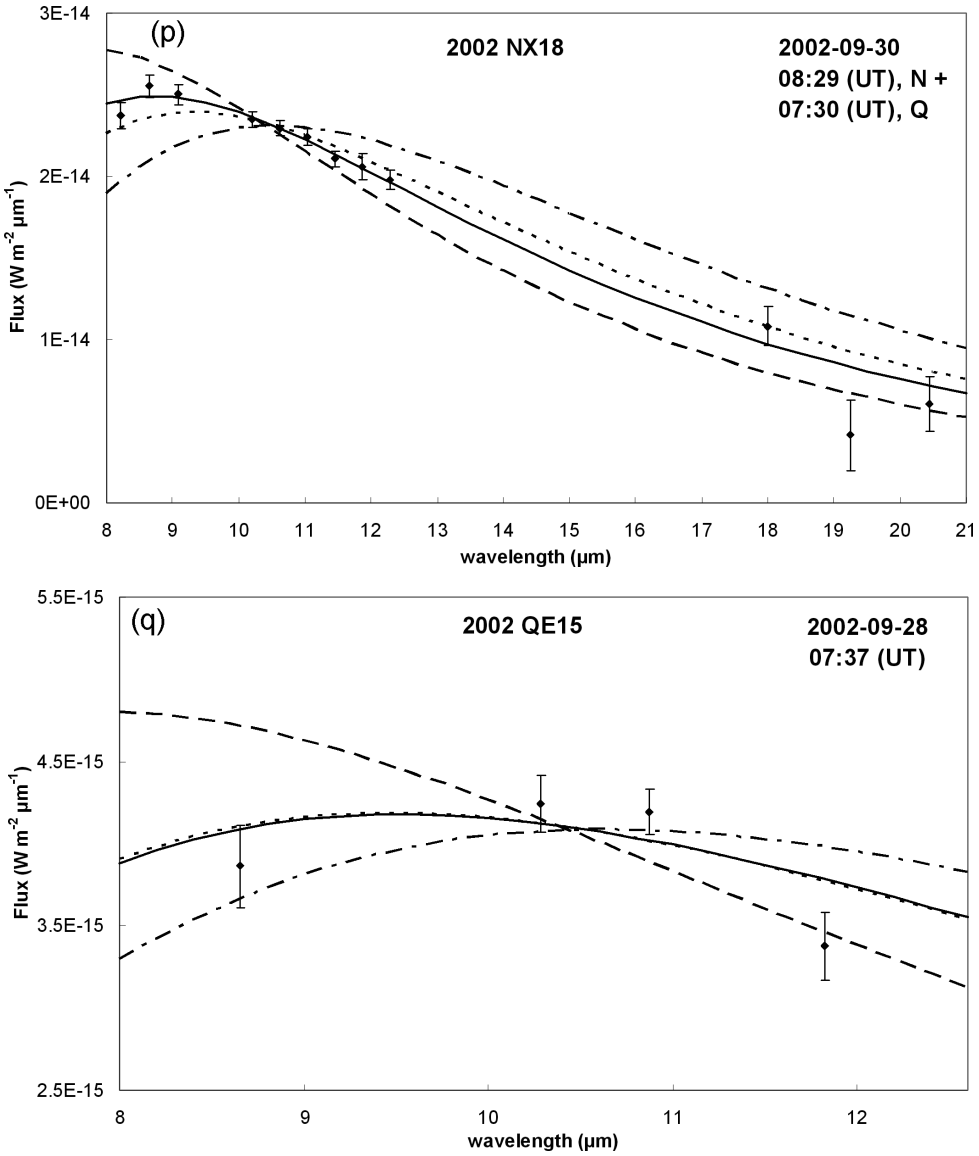

Fig. 2. Standard Thermal Model (STM, long-dashed line), Fast Rotating Model (FRM, dash–dot line), Near Earth Asteroid Thermal Model with default η (NEATM, dotted line) and NEATM with best-fit η (solid line) fits to calibrated binned Michelle spectra using lowN and lowQ gratings (September UKIRT observations) and reduced broadband observations using Michelle in imaging mode (March UKIRT observations). The weighted best fits are those that minimise $\sum[F_n(\text{obs}) - F_n(\text{mod})/\sigma_n]^2$ where $F_n(\text{obs})$ are the observed apparent fluxes, $F_n(\text{mod})$ are the model fluxes at that wavelength, and σ_n are the statistical uncertainties in the binned fluxes, resulting in a unique diameter and albedo for a given visual H magnitude. The derived effective diameters and albedos corresponding to (a) to (q) are listed in Table 2, as well as the visual H magnitude used, the best-fit η for each object, and the default η for those spectra based upon their phase angle (see Section 4). The Q spectra for (6455) 1992 HE, 2000 ED_{104}, taken in September are lightcurve corrected to the time of the N-band observation, assuming the thermal and visual lightcurves correspond.

taken at 10:30 UT (midpoint of exposure) for a single binned value, and binned over a wider range as described in Section 2.2. Figures 2(f) and 2(g) show the same 30 September N-band spectrum combined with the second Q-band spectrum taken at 11:01 UT. The Q-band spectra are lightcurve corrected to the magnitude of the asteroid at the time of the N-band spectrum, assuming that the thermal infrared and visual lightcurves coincide.

The thermal model fits for the March 2002 infrared photometry (Fig. 2(a)) are in excellent agreement with those for the September 28 thermal infrared N-band spectrum (Fig. 2(b)), indicating that these two techniques are consistent with each other.

Lightcurve correction of 30 September Q-band data placed the first (10:30 UT) Q-band spectrum very close to the NEATM best-fit η curve (Fig. 2(d) and 2(e), solid line), indicating that the absolute flux calibration was good enough to combine results from the two filters. The second Q-band spectrum (Figs. 2(f) and 2(g)) has lower fluxes. The NEATM fit shown in Fig. 2(e) was chosen as the 30 September contribution to calculating the adopted p_v and D_{eff} because the 10:30 UT Q-band spectrum is most consistent with the N-

Table 2
Measured albedos and effective diameters

Object/date	STM		FRM		NEATM default η			NEATM fitted/chosen η			Adopted results				H_v (mag)	$\alpha°$	Fig. 2	Comments
	p_v	$D_{\rm eff}$ (km)	p_v	$D_{\rm eff}$ (km)	η	p_v	$D_{\rm eff}$ (km)	η	p_v	$D_{\rm eff}$ (km)	p_v		$D_{\rm eff}$ (km)					
(6455) 1992 HE											**0.26**	**±0.08**	**3.55**	**±0.5**	14.32			
2002-03-22	0.27	3.52	0.088	6.14	1.0	0.23	3.83	**0.80**	**0.28**	**3.43**					14.32	22	(a)	Michelle imaging mode; rot. phase not known, lc. amp. < 0.1
2002-09-28	0.22	3.70	0.082	6.10	1.0	0.19	3.97	**0.79**	**0.24**	**3.55**					14.41	31	(b)	Rot. phase = 0.64
2002-09-30	0.18	4.16	0.062	7.10	1.0	0.16	4.48	0.57	0.27	3.43					14.38	28	(c)	N (rot. phase = 0.51)
	0.18	4.16	0.064	7.02		0.16	4.48	0.57	0.27	3.42					14.38		(d)	N + 10:30 (UT) 1Q (rot. phase = 0.84), lc. corrected to N-filter obs.
	0.18	4.16	0.062	7.08	1.0	0.16	4.48	**0.57**	**0.27**	**3.43**					14.38		(e)	N + 10:30 (UT) Qs, lc. corrected to N-filter obs.
								0.80	0.20	4.00					14.38			As above using mean η
	0.18	4.15	0.063	7.04	1.0	0.16	4.47	0.52	0.29	3.30					14.38		(f)	N + 11:01 (UT) 1Q (rot. phase = 0.18), lc. corrected to N-filter obs.
								0.53	0.28	3.33					14.38		(g)	N + 11:01 (UT) Qs, lc. corrected to N-filter obs.
1999 HF_1								**1.68**			**0.18**	**±0.07**	**3.73**	**+1.0 −0.5**	14.60			Mean mag. from Pravec (personal communication) err. ±0.5 mag
2002-03-22	0.34	2.72	**0.24**	**3.27**	1.5	0.13	4.46	**1.68**	**0.11**	**4.74**						91	(h)	Michelle imaging mode, Not lc. corrected, but low lc. amp. ±0.12 mag from Pravec (personal communication).
2000 ED_{104}								**1.69**			**0.18**	**+0.12 −0.08**	**1.21**	**±0.2**	17.10			Mean mag. from JPL Horizons, err. ±0.5 mag, 1 mag lc. amp.
2002-09-29	0.41	0.79	0.21	1.10	1.5	0.22	1.08	**1.80**	**0.18**	**1.18**						60	(i)	
2002-09-30	0.32	0.89	0.17	1.22	1.5	0.18	1.20	**1.57**	**0.17**	**1.23**						60	(j)	
2002 HK_{12}								**2.75**			**0.24**	**+0.25 −0.11**	**0.62**	**±0.2**	18.22			1.5 mag lc. amp.
2002-09-28	0.72	0.46	0.31	0.70	1.0	0.64	0.49	**2.75**	**0.24**	**0.80**					17.67	33	(k)	Rot. phase = 0.38, H_v value used disc. Section 3.3
2002 NX_{18}								**1.17**			**0.031**	**±0.009**	**2.24**	**±0.3**	17.63			
2002-09-27	0.049	1.79	0.022	2.66	1.5	0.027	2.43	**1.18**	**0.034**	**2.13**						52	(l)	
2002-09-29	0.051	1.76	0.023	2.63	1.5	0.027	2.42	2.19	0.017	3.02						53	(m)	Cirrus on 29 September
2002-09-30	0.040	1.99	0.018	2.95	1.5	0.021	2.73	**1.17**	0.028	2.38						54	(n)	N only
	0.040	1.99	0.018	2.95	1.5	0.021	2.73	**1.19**	0.027	2.40							(o)	N + 1Q, not lc. corrected but lc. amp. = 0.3 mag
	0.040	1.99	0.018	2.94	1.5	0.021	2.73	**1.16**	**0.028**	**2.37**							(p)	N + Qs
2002 QE_{15}								**1.53**			**0.15**	**+0.08 −0.06**	**1.94**	**±0.4**	16.21			Mean mag. from JPL Horizons, err. ±0.5 mag
2002-09-28	0.30	1.39	0.15	1.94	1.5	0.16	1.92	**1.53**	**0.15**	**1.94**						62	(q)	

Notes. Unless otherwise indicated, effective diameters and albedos are based on thermal model fits to 8–12.5 μm N-band data (Fig. 2). H magnitudes given on "object" rows are mean visual magnitudes, from JKT observations described in Section 3 in the case of (6455) 1992 HE, 2002 HK_{12} and 2002 NX_{18} or as described in the notes column. If H magnitude is left blank on the "date" rows, the mean H magnitude was used in the thermal fitting. In the cases of the September UKIRT observations of (6455) 1992 HE and 2002 HK_{12}, the rotational phases are known, and the corresponding H magnitudes used in the thermal fit are given on the "date" row. Values in bold are averaged for each object to provide the adopted p_v and $D_{\rm eff}$ (also in bold). Errors in the adopted p_v and $D_{\rm eff}$ are discussed in Section 4.

band spectrum, and it is taken closer in time than the 11:01 UT spectrum.

The 22 March and 28 September spectra (Figs. 2(a) and 2(b), solid line) both have very similar best-fit beaming parameters $\eta = 0.80$ and $\eta = 0.79$, respectively. But the 30 September spectrum has $\eta = 0.57$ (Figs. 2(c), 2(d), and 2(e), solid line). We have checked the calibration carefully, for example by trying different ratio stars, but the discrepancy remains. It could be that the weather, such as very light cirrus, affected the shape of the spectrum through wavelength-dependent absorption. However, the derived p_v and $D_{\rm eff}$ for 30 September ($p_v = 0.27$, $D_{\rm eff} = 3.43$ km) is very close

to that derived for 22 March ($p_v = 0.28$, $D_{\rm eff} = 3.43$ km) whereas if we set $\eta = 0.80$, the NEATM fit for 30 September has $p_v = 0.20$ and $D_{\rm eff} = 4.00$ km which is less consistent (although still within the 30% and 15% uncertainty for p_v and $D_{\rm eff}$, respectively). Delbó et al. (2003) found a conservative 20% uncertainty for a measurement of η based on the reproducibility of η for those objects for which more than one measurement is available, so the fitted beaming parameters are a little outside those limits (± 0.16). It is possible that it is a genuine effect, and that the beaming parameter varies on different parts of the asteroid due to changing surface characteristics, such as the extent of regolith or surface roughness, that affect the thermal inertia or emission. The midpoint of the 28 September N spectrum was at rotational phase 0.51, with reference to Fig. 1(a), whereas for 30 September it was at rotational phase 0.64.

All of the model fits to (6455) 1992 HE thermal IR spectra show that the FRM (dash–dot line) is not a good fit and the STM (dashed line) is an excellent fit. The adopted results are $p_v = 0.26 \pm 0.08$ and $D_{\rm eff} = 3.55 \pm 0.53$ km at the mean visual magnitude, $D_{\rm eff} = 3.73 \pm 0.56$ km at lightcurve maximum. The NEATM best-fit $\eta = 0.72$ (solid line) is very close to the STM value $\eta = 0.756$. A low near-STM beaming parameter even at a moderate phase angle ($\alpha = 22°, 30°$) suggests considerable beaming in the sunward direction due to surface roughness. Since we have found that (6455) 1992 HE is a relatively fast rotator, if it had any significant thermal inertia the beaming parameter would be greater than one (see Section 1). This indicates that (6455) 1992 HE has low thermal inertia implying a "dusty" regolith-covered surface. The value of $p_v = 0.26$ is consistent with its S-class taxonomic designation (Bus and Binzel, 2002).

4.2. 1999 HF_1

Figure 2(h) shows the thermal model fits for the 22 March thermal infrared photometry. We have no lightcurve correction for the observations, but the lightcurve amplitude is relatively small, < 0.23 (Pravec, personal communication, 2003). The STM (dashed line) is not a good fit; this is not surprising since the STM phase correction is not reliable at the phase angle the object was observed, $\alpha = 91°$. The FRM (dash–dot line) is better, but the NEATM with default $\eta = 1.5$ (dotted line) and fitted $\eta = 1.68$ (solid line) are both good fits. It is not known if the NEATM is reliable at such high phase angles; since the phase correction assumes zero emission on the night side, any body with significant thermal inertia will find the phase correction is not an adequate approximation at high phase angles. The adopted solution estimates p_v and $D_{\rm eff}$ by taking the average of the FRM and NEATM fits: $p_v = 0.18 \pm 0.07$, $D_{\rm eff} = 3.73\ (+1.0, -0.5)$ km at the mean visual magnitude, $D_{\rm eff} < 3.84\ (+1.0, -0.5)$ km at lightcurve maximum (from the limit of the lightcurve amplitude). 1999 HF_1 is a binary asteroid based on lightcurve characteristics (Pravec et al., 2002); the effect of this on thermal model fitting and the relative contribution of each component to observed fluxes is unknown. Pravec et al. found that 1999 HF_1 belongs to the X-type taxonomic class as defined by Bus and Binzel (2002), i.e., it is spectrally degenerate, and is either an E, M, or a P-type asteroid. From our estimated p_v we can say that the spectrally dominant component is not a P-type, but could still be either an E- or an M-type.

4.3. 2000 ED_{104}

Figures 2(i) and 2(j) show thermal fits to 29 September and 30 September N-band spectra, respectively. Although there was cirrus on the second half of 29 September resulting in noisy data (not presented here) for Asteroids (6455) 1992 HE and (433) Eros, early observations made of 2000 ED_{104} and 2002 NX_{18}, when the weather was clearer, agree with observations on other nights.

The STM (dashed line) is not a good fit, perhaps due to the high phase angle of observation. The NEATM with default $\eta = 1.5$ (dotted line) gives a better fit than the FRM (dash–dot line). The thermal infrared flux was close to the detection threshold, hence the spectral resolution is low, and consequently the fitted η is rather uncertain. Since the lightcurve amplitude is greater than 1 mag, the difference in measured albedo and diameter between 29 and 30 September, based on a value of the visual magnitude derived from the catalogued $H_v = 17.10 \pm 0.5$, can be attributed to the changing brightness (and therefore projected area, i.e., the assumption that the object is a sphere is not reasonable). The adopted $p_v = 0.18\ (+0.11, -0.06)$ is an intermediate albedo consistent with taxonomic classes such as S, M, Q, R, and V. $D_{\rm eff} = 1.21 \pm 0.2$ km at the mean visual magnitude.

4.4. 2002 HK_{12}

2002 HK_{12} was the object with the lowest thermal flux we were able to measure successfully. Figure 2(k) shows the thermal model fits to the 28 September N-band spectrum. The STM (dashed line) and NEATM with default $\eta = 1.0$ (dotted line) do not fit well. The NEATM fit (solid line) has an unusually high beaming parameter $\eta = 2.75$, and is a similar shape to the FRM (dash–dot line); both fit the spectrum well. The high beaming parameter at a moderate phase angle ($\alpha = 33°$) and good fit of the FRM suggests that 2002 HK_{12} may have a surface with significant thermal inertia, such as bare rock. The adopted $p_v = 0.24\ (+0.25, -0.11)$ is an intermediate albedo consistent with taxonomic classes such as S, M, Q, R, and V. $D_{\rm eff} = 0.62 \pm 0.2$ km at the mean visual magnitude.

4.5. 2002 NX_{18}

Figures 2(l), 2(m), and 2(n) show thermal fits to N-band spectra on 27, 29, and 30 September, respectively. The spectra on all three nights are of high spectral resolution, binned over 0.25 μm wavebands for the lowN grating on 27 and 29

September, and over 0.27 μm wavebands for the lowN grating on 30 September. Figures 2(o) and 2(p) show thermal fits to the 30 September N-band spectrum combined with the Q-band spectrum taken on the same night, binned as a single value and over a larger wavelength range as described in Section 2.2.

Because we do not have a unique solution for the rotational period of 2000 NX_{18} it was not possible to lightcurve correct the Q-band to the N-band data. The visual observations were used to supply the H_v magnitude used in the thermal model fits. As described in Section 3.3 the lightcurve amplitude is 0.23, which is not large, so the error in p_v and $D_{\rm eff}$ is dominated by the model-fitting.

The STM (dashed line) does not fit well, as would be expected given the large phase angle of observation ($\alpha = 53°$). The FRM (dash–dot line) fits badly on 27 September (Fig. 2(l)) and 30 September (Figs. 2(n), 2(o), and 2(p)), but fits well on 29 September (Fig. 2(m)). The $\eta = 1.18$ fit for NEATM on 27 September is in very close agreement with $\eta = 1.16$ on 30 September. We regard the NEATM with fitted η as reliable on 27 September and 30 September, and hence these fits were used to calculate the adopted p_v and $D_{\rm eff}$.

The 29 September spectrum has a different shape from the other two nights, such that the FRM gives a good fit, and the NEATM fit has a much higher beaming parameter $\eta = 2.19$. The weather later in the night on 29 September was affected by cirrus, so it is possible that the wavelength-dependent calibration with the standard star affected the shape of the spectra more than is typical due to differing atmospheric absorption at different wavelengths. We regard the NEATM fit on 29 September as being unreliable.

We were unable to obtain enough optical observations to derive a unique solution for the rotational period of 2002 NX_{18} (Section 3.3 and Figs. 1(c) and 1(d)) although the visual magnitude was used to estimate H_v for the thermal models. Therefore we were not able to lightcurve correct the thermal spectra in the way described for (6455) 1992 HE. It is possible that the higher beaming parameter measured on 29 September is due to differing thermal properties at different parts of the asteroid surface. However, if either of the two most likely solutions for the rotational period ($P = 7.602$ h and $P = 9.040$ h) are correct then the observations on 27 and 29 September are on the same hemisphere (for $P = 7.602$ h, rotational phase 0.39 and 0.49 on 27 and 29 September, respectively; for $P = 9.040$ h, rotational phase 0.21 and 0.34).

The adopted $p_v = 0.031 \pm 0.009$ is a low albedo consistent with taxonomic classes such as B, C, D or P. $D_{\rm eff} = 2.24 \pm 0.3$ km at the mean visual magnitude, $D_{\rm eff} = 2.40 \pm 0.3$ km at lightcurve maximum.

4.6. 2002 QE_{15}

Figure 2(q) shows the thermal model fits to the 28 September N-band spectrum. None of the thermal models fit well because of the large scatter due to the low thermal flux. The best-fit NEATM has a beaming parameter of $\eta = 1.53$. For the other asteroids we adopt an estimate of the uncertainty in measurement of η at 20% based on the reproducibility for those objects for which there is more than one measurement from independent data sets. For 2002 QE_{15}, because of the large scatter, we increase the uncertainty to 50%. The adopted $p_v = 0.15$ ($+0.08, -0.06$) is an intermediate albedo consistent with taxonomic classes such as S, M, Q, R, and V. $D_{\rm eff} = 1.94 \pm 0.4$ km at the mean visual magnitude.

5. Discussion

Of the six NEAs with measured albedos and diameters presented here, only (6455) 1992 HE and 2002 HK_{12} were observed at a phase angle below 45°. The other four objects all have phase angles between 51° (2002 NX_{18}) and 91° (1999 HF_1). Figure 3 shows a plot of beaming parameter versus phase angle from Delbó et al. (2003), with the values derived in this paper overlaid. Delbó et al. found a trend of increasing beaming parameter with phase angle. Our values are consistent with this trend. The 1999 HF_1 point suggests that the trend continues to higher phase angles than have been observed previously.

The NEATM allows the beaming parameter to be adjusted to fit the apparent colour temperature implied by the spectra. At low phase angles, for large main-belt asteroids with a low thermal inertia, typically covered with a mature dusty regolith, the beaming parameter can be expected to be less than 1 as there is enhanced emission in the sunward direction due to surface roughness. Hence the STM gives good fits with $\eta = 0.756$. At mid- to high-phase angles for such objects, the beaming parameter could be expected to be higher, since the apparent colour temperature would be lower for energy to be conserved, because there is "missing" thermal flux being sent in the sunward direction.

The exception in Fig. 3 is 2002 HK_{12}, which appears to join a group of four other anomalous objects. Like these objects, the FRM for 2002 HK_{12} is also a good fit. One interpretation of the fact that many NEAs appear to have a value of $\eta \geqslant 1$ is that beaming due to roughness may be less than that of other Solar System bodies, and that, due to high thermal inertia and/or fast rotation rates, the temperature distributions around the body are smoothed and there is significant thermal emission on the night side. Higher thermal inertia and rotation causes η to increase. Using the relation derived by Spencer et al. (1989), a rough estimate of the surface thermal inertia from measured values of η can be obtained. For example, Harris et al. (1998) found high values for some smaller near-Earth asteroids that are characteristic of pure rock. The η-value found for 2002 HK_{12} of 2.75 indicates an unrealistically high thermal inertia $> 5000\ \mathrm{J\,m^{-2}\,s^{-0.5}\,K^{-1}}$. An explanation of η-values purely in terms of thermal inertia and surface roughness is probably an oversimplification. Delbó et al. (2003) pointed out the disconcerting fact that no

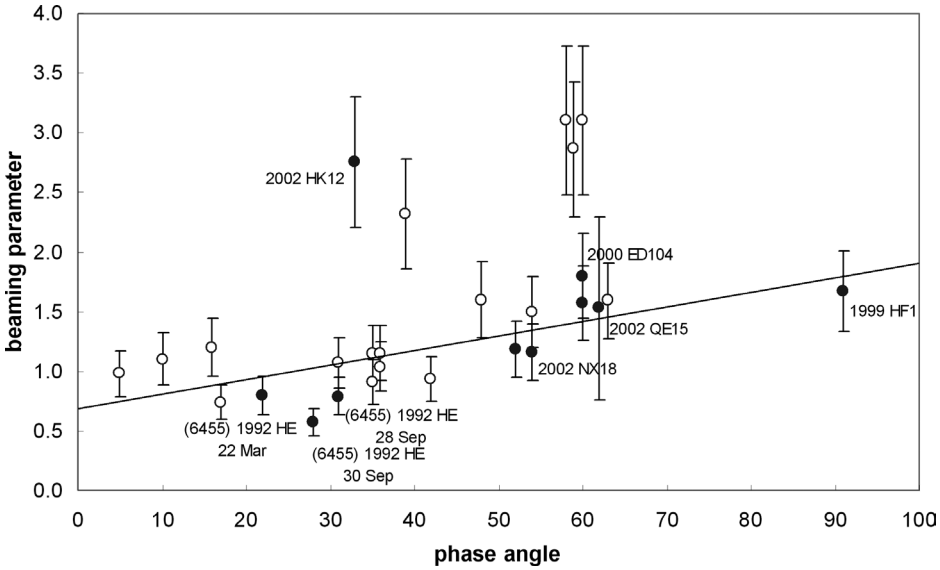

Fig. 3. The relationship between phase angle (α) and fitted beaming parameters (η). Open circles are from Delbó et al. (2003) and solid circles are derived in this paper and given in Table 2. The line shows a linear fit excluding objects with $\eta > 2.0$ ($\eta = 0.69 + 0.012\alpha$). The error bars represent a 20% uncertainty based on the reproducibility for those objects for which there is more than one measurement from independent data sets, except for 2002 QE_{15} where the uncertainty is 50% (Section 4.6).

high-η objects are observed at moderate or low phase angles. The 2002 HK_{12} point is at a lower phase angle than the other high-η objects. They suggest two different explanations, beyond the fact that a statistically significant number of objects have not yet been observed. (i) Two of the high-η objects are known to be binaries. Near-Earth binaries may have unusually rough surfaces because of possible disruption of the rubble piles, from which they are thought to be constituted, when passing close to a planet. As a result they would have a high degree of beaming in the sunward direction due to surface roughness, and consequently a lower apparent temperature distribution at high phase angles. (ii) NEAs can often be elongated, so shape or shadowing effects may be more pronounced at high phase angles. 2002 HK_{12} could be an example of (ii), since it has a lightcurve amplitude of 1.5 mag, indicating that it is an elongated asteroid.

The NEATM phase correction models the asteroid as a smooth sphere, assuming Lambertian emission, and calculates the thermal flux from the sunlit portion visible to the observer only, thereby assuming zero emission from the night side. Objects with significant thermal inertia will have non-negligible thermal emission on their night side; at higher phase angles the effect of omitting the night side emission will be more significant. By assuming zero emission, all the observed thermal flux has to come from the sunlit side. To account for the low colour temperature for the observed thermal flux, higher best-fit values of η are found. This may contribute to the general trend of increasing η with higher phase angles as well as to the high beaming parameters of the anomalous objects. If the thermal emission on the night side was included in the model, e.g., Green et al. (1985), who used a modified projected model that defined a non-zero dark side temperature distribution for (3200) Phaethon, then this might lead to clarification of the effects on η at high phase angle and the physical interpretation of best-fit beaming parameters. With the current wide scatter in measured beaming parameters at high phase angle, the use of a default $\eta = 1.5$ could be unsafe, although it is interesting that in the cases for 1999 HF_1 which is a binary asteroid, and for 2000 ED_{104} which has a large lightcurve amplitude and is therefore presumably very elongated, they both fit well on the trend shown in Fig. 3. The situation may be clarified when there is a greater dataset of NEAs observed in the thermal infrared at several different phase angles.

It may be instructive to point out the observational selection effects that resulted in the objects that were observed. Before conducting an observing run, targets were selected on the basis of their visual magnitudes. This selects against small, low-albedo objects. For a given optical limit, objects may be large, low albedo, or small, high albedo. Large, low albedo objects will be easier to detect in the infrared. In trying to measure their thermal flux, the prioritised objects that were small, high albedo, were not bright enough for Michelle, on UKIRT, to measure the thermal flux (2002 HK_{12} was near the threshold of where a sensible flux could be measured), and so were discarded. The end result is that small asteroids are selected against. There is a tendency at this stage to obtain meaningful results only for large, low-albedo objects such as 2002 NX_{18}.

6. Conclusions

We have derived the geometric albedos and effective diameters (all given at mean visual magnitude) of six different NEAs, using the STM, FRM, NEATM with default beaming

parameter η appropriate to the phase angle of observation, and also with a best-fit η, applied to thermal infrared photometry and spectrophotometry.

We found the geometric albedo of (6455) 1992 HE to be $p_v = 0.26 \pm 0.08$, effective diameter $D_{\rm eff} = 3.55 \pm 0.5$ km using NEATM, with a best-fit beaming parameter $\eta = 0.80$ at a phase angle of 22°, and an average $\eta = 0.68$ at 31°. This is consistent with its S taxonomic class. From JKT observations, we derived a rotational period $P = 2.736 \pm 0.002$ h, an absolute visual magnitude $H = 14.32 \pm 0.24$, and a lightcurve amplitude = 0.21. The relatively fast rotation rate, coupled with a bad fit for the FRM and a low fitted η, indicates that (6455) 1992 HE is a low thermal inertia, extended-regolith, "dusty" object.

It is not possible to clarify which model is to be preferred for 1999 HF_1, since it is not clear how reliable NEATM is at the high phase angle of observation ($\alpha = 91°$). The albedo is estimated as an average of the FRM and NEATM fits: $p_v = 0.19 \pm 0.07$ and $D_{\rm eff} = 3.73$ (+1.0, −0.5) km. It is known to be a spectrally degenerate X-type asteroid (E, M or P); the derived albedo indicates that it is not a P-type.

2000 ED_{104} has a moderate albedo $p_v = 0.18$ (+0.12, −0.08), $D_{\rm eff} = 1.21 \pm 0.2$ km, and a best-fit $\eta = 1.69$ at $\alpha = 60°$.

2002 HK_{12} has a moderate albedo $p_v = 0.24$ (+0.25, −0.11), $D_{\rm eff} = 0.62 \pm 0.2$ km, and an unusually high best-fit $\eta = 2.75$ at $\alpha = 33°$. The FRM was also a good fit. This suggests that 2002 HK_{12} may have a surface with a high thermal inertia, such as bare rock. From JKT observations we derived an absolute visual magnitude $H = 18.22$ (+0.37, −0.30).

2002 NX_{18} has an unusually low albedo $p_v = 0.031 \pm 0.009$ and $D_{\rm eff} = 2.24 \pm 0.3$ km, with an average fitted $\eta = 1.18$ at $\alpha = 53°$.

2002 QE_{15} has a moderate albedo $p_v = 0.15$ (+0.08, −0.06), $D_{\rm eff} = 1.94 \pm 0.4$ km, and a best-fit $\eta = 1.53$ at $\alpha = 62°$.

Acknowledgments

The Jacobus Kapteyn Telescope was operated on the island of La Palma by the Royal Greenwich Observatory in the Spanish Observatorio del Roque de los Muchachos of the Instituto de Astrofisica de Canarias. The United Kingdom Infrared Telescope is operated by the Joint Astronomy Centre on behalf of the U.K. Particle Physics and Astronomy Research Council. We thank the reviewers Petr Pravec, for supplying lightcurve parameters and a useful critique of the optical observations, and Marco Delbó, for help with thermal modelling calculation and interpretation. We also thank Tom Kerr and Paul Hirst for their invaluable troubleshooting of ORAC-DR, and Alan Harris (DLR) for helpful comments and suggestions on thermal modelling. The work of S.D. Wolters was supported by the Particle Physics and Astronomy Research Council.

References

Bowell, E., Hapke, B., Domingue, D., Lumme, K., Peltoniemi, J., Harris, A.W., 1989. Application of photometric models to asteroids. In: Binzel, R.P., Gehrels, T., Matthews, M.S. (Eds.), Asteroids II. Univ. of Arizona Press, Tucson, pp. 524–556.

Bus, S.J., Binzel, R.P., 2002. Phase II of the small main-belt asteroid spectroscopic survey. Icarus 158, 146–177.

Delbó, M., Harris, A.W., Binzel, R.P., Pravec, P., Davies, K.J., 2003. Keck observations of near-Earth asteroids in the thermal infrared. Icarus 166, 116–130.

Fowler, J.W., Chillemi, J.R., 1992. IRAS asteroid data processing. In: The IRAS Minor Planet Survey. Phillips Laboratory, Hanscom AF Base, MA, pp. 17–43.

Green, S.F., McBride, N., 1998. Photometry techniques—report of splinter meeting. In: Fitzsimmons, A., Jewitt, D., West, R.M. (Eds.), ESO Workshop. pp. 57–60.

Green, S.F., Meadows, A.J., Davies, J.K., 1985. Infrared observations of the extinct cometary candidate minor planet (3200) 1983 TB. Mon. Not. R. Astron. Soc. 214, 29P–35P.

Harris, A.W., 1998. A thermal model for near-Earth asteroids. Icarus 131, 291–301.

Harris, A.W., Harris, A.W., 1997. On the revision of radiometric albedos and diameters. Icarus 126, 450–454.

Harris, A.W., Davies, J.K., Green, S.F., 1998. Thermal infrared spectrophotometry of the near-Earth Asteroids 2100 Ra–Shalom and 1991 EE. Icarus 135, 441–450.

Landolt, A.U., 1992. UBVRI photometric standard stars in the magnitude range $11.5 < V < 16.0$ around the celestial equator. Astron. J. 104, 340–491.

Lebofsky, L.A., Spencer, J.R., 1989. Radiometry and thermal modeling of asteroids. In: Binzel, R.P., Gehrels, T., Matthews, M.S. (Eds.), Asteroids II. Univ. of Arizona Press, Tucson, pp. 128–147.

Lebofsky, L.A., Sykes, M.V., Tedesco, E.F., Veeder, G.J., Matson, L.D., Brown, R.H., Gradie, J.C., Feierberg, M.A., Rudy, R.J., 1986. A refined "standard" thermal model for asteroids based on observations of 1 Ceres and 2 Pallas. Icarus 68, 239–251.

Morrison, D., 1977. Radiometric diameters of 84 asteroids from observations in 1974–1976. Astrophys. J. 214, 667–677.

Pravec, P., Šarounová, L., Hicks, M., Rabinowitz, D., Wolf, M., Scheirich, P., Krugly, Y., 2002. Two periods of 1999 HF_1—another binary NEA candidate. Icarus 158, 276–280.

Rieke, G.H., Lebofsky, M.J., Low, F.J., 1985. An absolute photometric system at 10-μm and 20-μm. Astron. J. 90, 900–906.

Spencer, J.R., Lebofsky, L.A., Sykes, M.V., 1989. Systematic biases in radiometric diameter interpretations. Icarus 78, 337–354.

Tokunaga, A.T., 1984. A re-evaluation of the 20-μm magnitude system. Astron. J. 89, 172–175.

Tokunaga, A.T., 2000. Infrared astronomy. In: Cox, A.N. (Ed.), Allen's Astrophysical Quantities. The Athlone Press, Los Alamos, pp. 143–167.

Veeder, G.J., Hanner, M.S., Matson, D.L., Tedesco, E.F., Lebofsky, L.A., Tokunaga, A.T., 1989. Radiometry of near-Earth asteroids. Astron. J. 97, 1211–1219.